PROPERTIES OF GRAPHENE IN-PLANE HYBRID EMBRACING HEXAGONAL SHAPED HEXAGONAL-BORON NITRIDE (h-BN) ISLANDS AND VACANCY INDUCED MAGNETISM

Cem Özdoğan[a] and Nurten Akman[b]
[a] Izmir Katip Celebi University, Izmir, Turkey E-mail: cem.ozdogan@ikc.edu.tr
[b] Mersin University, İçel, Turkey E-mail: nurten.akman@gmail.com

Abstract

Hexagonal boron nitrate h-BN islands in hexagonal shape with defect in the form of single vacancy have been patterned in graphene layout. Energetics of ion implantation, defect formation, stability, electronic, and magnetic properties of graphene/(h-BN) in-plane hybrids are investigated through first principle calculations. We consider hexagonal islands in hexagonal supercells of graphene layout. The energetics of island implantation is discussed in detail. Formation energies point out that the island implantation could be even exothermic for all hybrids studied in this work. Effects of size on the stability, band gap, and magnetic properties of hybrids are studied particularly. Pristine hybrids are all non-magnetic and semiconducting whereas defective counterparts might become metallic and posses a modest magnetic moments.

Keywords: Graphene, in-plane hybrids, nanomagnetism, nanopatterning

1. Introduction

Each graphene (G) and hexagonal boron nitride (h-BN) are very promising two dimensional (2D) materials with honeycomb structure [1,2]. Easy control of their electronic and transport properties makes these conducting or insulating 2D systems quite desirable [2]. The symmetry between two sublattices of the honeycomb structure makes graphene a gapless semiconductor. On the other hand, h-BN without having such symmetry is a wide band gap (5.5 eV) insulator [3]. It is already shown that the band gap tune up in these materials can be accomplished by reducing their dimension to form a nanoribbon [4], hydrogenization [5] and applying an external field [6].

Graphene and h-BN can easily hybridize to form a graphene/ h-BN (GBN) hybrid material due to their small (~1.6%) lattice mismatch. In-plane and stacked GBN hybrid materials have been constituted on a Cu substrate by controlling the synthesis conditions of the CVD method [7,8]. It is already known that graphene becomes semiconductor when its structure is modified by means of defects [9] or by doping with B and N atoms or when it embraces a small-size h-BN domain [10-14]. GBN nanosheets consisting of a h-BN domain in a graphene lattice were studied by using the ab initio
DFT, and opening of a band gap E_g by varying the size of h-BN domain was observed [15, 16]. Tunability of the electrical properties of GBN hybrids has also been discussed from the experimental point of view [17].

Defective systems are even attractive mediums in the scope of engineered electronics. Defect dynamics in graphene and graphene-likematerials, such as h-BN and transition metal dichalcogenide, have been studied in detailwith the electronmicroscopy techniques [18]. It is known that experimentalists could create magnetic moments at the edges of graphene by edge type defects or in graphene by point defects. An intrinsic or artificial vacancy can be produced experimentally during the synthesis process or later by the irradiation, respectively. Mono vacancy in a free-standing graphene might also lead to a magnetism by splitting the localized state of defect into two density of states (DOS) [19].

Our aim in the present study is to investigate the electronic and magnetic properties of GBN nano pristine and defective hybrids consisting of a various sized hexagonal h-BN island within the framework of DFT. We explore size effects of the h-BN island on the energetics, energy band gap, and magnetic properties of GBN hybrids together with energetics of ion implantation and defect formation. We investigate how the electronic and magnetic properties of GBN hybrids change when a single vacancy is located at various sites.

2. Computational Method

Our numerical calculations were performed by using first-principles within the framework of the DFT [20]. We adopted the generalized gradient approximation (GGA) for the exchange-correlation potential together with the Perdew-Wang parametrization (PW91) [21,22]. For structural optimizations, electronic and density of states (DOS) calculations, we used the Vienna Ab Initio Simulation Package (VASP, version 5.3) [23,24] employing the projected augmented wave (PAW) method [25,26].

In our study we consider a graphene layout involving an h-BN island (see Tables 1 and 2). After we obtained the ground state geometries of the pristine graphene and h-BN nanosheets (9x9 supercell), we defined and optimized the hybrid structures involving an hexagonal h-BN island. Concerning vacancy, we just ejected a C (B or N) atom residing at the interface or in the graphene layout or in the island of previously optimized hybrid. For a given GBN hybrid, 7 different mono vacancies were proposed at most. Explicit definitions of notations for vacancy types are stated in Section 3.5.

In order to avoid any residual interaction along the z-direction, the in-plane system is separated from its replicas by around 14 Å. The geometries were

optimized into their instantaneous ground states by using the conjugate-gradient (CG) algorithm. The Brillouin zone was sampled by using a Γ-point centered
Monkhorst-Pack grid.

Optimum k-point mesh to be used in the geometry relaxation calculations is converged as the changes in total energy is at least below 10 meV/atom. After having the optimum k-point meshes, geometries of the hybrid nanosheetswere fully optimized in a self-consistent manner. Same k-point meshes as for the pristine GBN hybrids were sampled during our calculations of the defective hybrids. After the atomic relaxation, a static self-consistent calculation was performed to obtain the charge density and total energies of the systems. Our criterion for energy convergence was 10^{-5}, and for total force on each atom was 0.01 eV/atom. We performed spin unpolarized (NSP) and spin polarized (SP) calculations for each hybrid structure to determine their ground states and magnetic moments. For magnetic systems collinear, SP DFT calculations were performed in all steps described above.

3. Results

In this section we will discuss the energetics of island implantation, defect formation, electronic, and magnetic properties of graphene, h-BN, and GBN hybrid systems. The difference between the NSP and SP total energies is defined as the magnetization energy ΔE_M,

$$\Delta E_M = E_{\mathrm{NSP}} - E_{\mathrm{SP}}\,. \qquad (1)$$

Positive ΔE_M signifies that the system has a SP ground state, otherwise it prefers a NSP ground state.

3.1. Energetics of Island Implantation

Implantation of hybrids through the solid state reactions between the graphene layout and the BN clusters can be sketched out as

$$\mathbf{G}_{162} + \mathbf{B}_Y + \mathbf{N}_Z \longrightarrow \mathbf{h\text{-}BN@G} + \mathbf{C}_{Y+Z}. \qquad (2)$$

Energy needed to break the local bonds of graphite and bulk h-BN is almost the same. Incident ion beam that impinges on the bulk sample supplies the energy required to break the local bonds of the samples. Although many reaction pathways is possible during a collision process, only some of them is highly probable. The formation energy ε_f is defined in equation 3. Extreme values of the formation energy are defined in equation 4. Chemical potentials are considered to be free reaction parameters, and hence they refer to either atomic or asymptotic bulk limits for both the incident and the sputtered structures. We calculated the formation energies ε_f at zero temperature and pressure.

$$\mathcal{E}_{\mathrm{f}} = (E_{\mathbf{h\text{-}BN@G}} + (Y+Z)\times\mu[\mathbf{C}]) - (E_{\mathbf{G}_{162}} + Y\times\mu[\mathbf{B}] + Z\times\mu[\mathbf{N}])\,. \qquad (3)$$

Here the chemical potential μ[*B*] (μ[*N*]) varies in between the free B (N) atom and the boron (nitrogen) bulk energies. Similarly, μ[*C*] is in between atomic carbon and graphite energies. Various formation scenarios might take place in the range of these extremes. We only calculated extremes of the formation energy, and discussed stability of the hybrids. Relations in Eqn. 4 provide the minimum and maximum formation energies of the hybrid embracing an h-BN island.

$$\begin{aligned}\mathcal{E}_{\mathrm{f_{min}}} &= (E_{\mathbf{h\text{-}BN@G}} + (Y+Z)\times\mu[\mathbf{C_{bulk}}]) - (E_{\mathbf{G}_{162}} + Y\times\mu[\mathbf{B_{atom}}] + Z\times\mu[\mathbf{N_{atom}}])\\ \mathcal{E}_{\mathrm{f_{max}}} &= (E_{\mathbf{h\text{-}BN@G}} + (Y+Z)\times\mu[\mathbf{C_{atom}}]) - (E_{\mathbf{G}_{162}} + Y\times\mu[\mathbf{B_{bulk}}] + Z\times\mu[\mathbf{N_{bulk}}]) \qquad (4)\end{aligned}$$

E_{G162} and $E_{h\text{-}BN@G}$ are the respective total energies of pristine graphene and graphene layout embracing an h-BN island. We calculated the chemical potentials of atoms and the bulk elements as: $\mu[B_{atom}]$=-0.26 eV, $\mu[B_{bulk}]$=-6.68 eV/atom (α-rhombohedral [27]), $\mu[N_{atom}]$=-3.00 eV, $\mu[N_{bulk}]$=-8.34 eV/atom ([28]), $\mu[C_{atom}]$=-1.19 eV, $\mu[C_{bulk}]$=-9.24 eV/atom (graphite). Extremes of the formation energies are collected in Table 1.

Table 1 Formation energies (Eqn. 4) for the hybrids displayed in Fig. 2. Formation energies per total number of atoms involved by the island are given in the last two columns.

Hybrid	Name	$\mathcal{E}_{\mathrm{f_{min}}}$ (eV)	$\mathcal{E}_{\mathrm{f_{max}}}$ (eV)	$\mathcal{E}_{\mathrm{f_{min}}}$ (eV)	$\mathcal{E}_{\mathrm{f_{max}}}$ (eV)
$C_{156}B_3N_3$	1h-BN(H)@G	−39.9	43.6	−6.65	7.27
$C_{138}B_{12}N_{12}$	7h-BN(H)@G	−166.0	168.2	−6.92	7.01
$C_{108}B_{27}N_{27}$	19h-BN(H)@G	−378.3	373.7	−7.01	6.92

The energetics prove that the reactions are typically endothermic ion implantation processes. But depending
on the initial and the final states of B, N, and C atoms, they might also be exothermic. Hence, ε_f values support our previous argument that the in-plane hybrids
might be synthesized under suitable experimental conditions.

As normalized with total number of doped atoms, minimumformation energy values (fifth column) gradually decrease with increasing island size. The formation energy evidently tends to approach the cohesive energy of graphite or bulk h-BN.

3.2. Energetics of Defect Formation

In this work, we will consider defective hybrids in the form of mono vacancy and defect formation energies of the hybrids are found as the following

$$E_{form}[D(i,q)] = E_{total}[D(i,q)] - E_{total}[D(0,q)] + \sum[n(i)*\mu(i)] \qquad (5)$$

where $E_{total}[D(i, q)]$ is the ground state total energy of the system with having i vacancy and with q charge,

$E_{total}[D(0, q)]$ is the total energy of the system with 0 vacancy and with q charge, n(i) is the number of vacancies of different atoms and μ(i) is the chemical potential of corresponding vacancy atom. In this study, we have single vacancy (i=1) and neutral charge defect (q=0).
Table 2 tabulates obtained defect formation energies and also summarizes all studied hybrids. The energetics prove that the reactions are typically endothermic vacancy formation processes. There is no any observed strict correlation between island size and defect formation energy. However, it could be stated as the defect formation energy tends to increase in general.

Table 2: Defect formation energies (Eqn. 5) for G, h-BN and defective hybrids.

System	Name	E_{total} (eV)	E_{form} (eV)
C_{162}	pristine	-1496.12	-
C_{161}	VC	-1479.28	7.60
$B_{81}N_{81}$	pristine	-1431.56	-
$B_{80}N_{81}$	VB	-1414.72	10.16
$B_{81}N_{80}$	VN	-1415.51	7.72
$C_{156}B_3N_3$	1h-BN(H)@G	-1490.39	-
$C_{156}B_2N_3$	1h-BN(H-VB_I)@G	-1476.97	6.73
$C_{155}B_3N_3$	1h-BN(H-VC_{I1})@G	-1476.00	5.15
$C_{155}B_3N_3$	1h-BN(H-VC_{I2})@G	-1474.43	6.72
$C_{155}B_3N_3$	1h-BN(H-VC_L)@G	-1473.48	7.67
$C_{156}B_3N_2$	1h-BN(H-VN_I)@G	-1475.02	7.03
$C_{138}B_{12}N_{12}$	7h-BN(H)@G	-1479.53	-
$C_{138}B_{11}N_{12}$	7h-BN(H-VB_i)@G	-1464.25	8.59
$C_{138}B_{11}N_{12}$	7h-BN(H-VB_I)@G	-1465.53	7.31
$C_{137}B_{12}N_{12}$	7h-BN(H-VC_{I1})@G	-1464.68	5.61
$C_{137}B_{12}N_{12}$	7h-BN(H-VC_{I2})@G	-1463.40	6.89
$C_{137}B_{12}N_{12}$	7h-BN(H-VC_L)@G	-1463.00	7.30
$C_{138}B_{12}N_{11}$	7h-BN(H-VN_i)@G	-1463.76	7.43
$C_{138}B_{12}N_{11}$	7h-BN(H-VN_I)@G	-1464.28	6.92
$C_{108}B_{27}N_{27}$	19h-BN(H)@G	-1463.57	-
$C_{108}B_{26}N_{27}$	19h-BN(H-VB_i)@G	-1447.83	9.06
$C_{108}B_{26}N_{27}$	19h-BN(H-VB_I)@G	-1448.65	8.23
$C_{107}B_{27}N_{27}$	19h-BN(H-VC_{I1})@G	-1448.37	5.96
$C_{107}B_{27}N_{27}$	19h-BN(H-VC_{I2})@G	-1447.31	7.03
$C_{107}B_{27}N_{27}$	19h-BN(H-VC_L)@G	-1446.54	7.80
$C_{108}B_{27}N_{26}$	19h-BN(H-VN_i)@G	-1447.66	7.57
$C_{108}B_{27}N_{26}$	19h-BN(H-VN_I)@G	-1448.31	6.92

3.3. Graphene and h-BN Sheets with Mono Vacancy

The ground state geometries of defective graphene and h-BN nanosheets are depicted in Fig. 1a-c. Calculated
ΔE_M, bandgap and magnetic moment values for graphene/h-BN and their corresponding mono vacancy
systems are tabulated in Table 3. Pristine nanosheets do not possess a magnetic moment and hence they are nonmagnetic structures. Calculated ΔE_M values for pristine graphene and h-BN are -3.2 and 0.4 meV, respectively. As expected, graphene is a semimetal at Γ point, and h-BN is an insulator with a direct band gap of 4.592 eV. Their energy band structures are respectively presented in Fig. 1g and 1h. A relevant discussion comparison with literature of these pristine sheets and non-defective hybrids having hexagonal and triangularshaped islands presented in our earlier work [29]. Mono vacancies were designated as VC, VB and VN for a missing C, B and N atom respectively.

The Fermi energy, E_F, of graphene with vacancy decreases while the shape of band structure for pristine
case is generally preserved by an up-shifting as seen in
Fig. 1d. States crossing the Fermi level make the system metallic. Some states due to dangling bonds occurs near to the E_F and leads to a small amount of

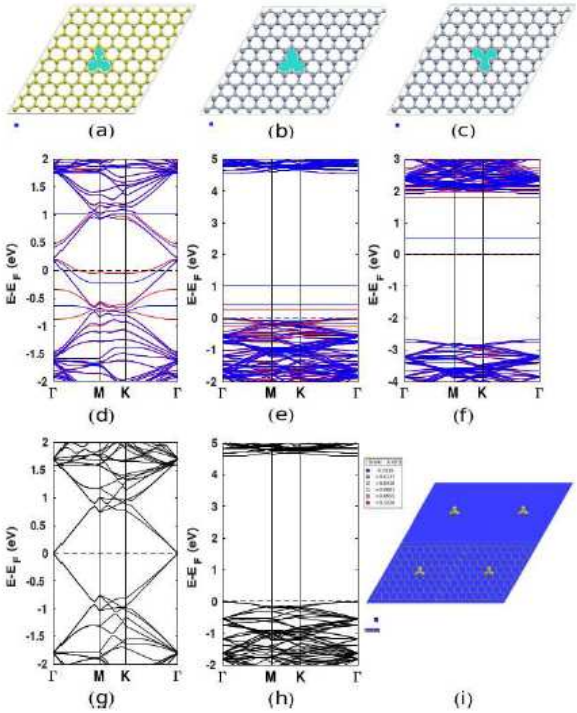

Figure 1. Optimized geometries for (a) carbon vacancy graphene (b) boron vacancy h-BN and (c) nitrogen vacancy h-BN nanosheets. The yellow, gray and light blue colors show respectively C, B, and N atoms. Electronic band structures of C, B, and N vacancy sheets are ordered in middle line through (d)-(f) respectively. Band structures of pristine graphene (g) and h-BN (h). Spin density of h-BN with N vacancy (i). It is plotted at contours of 0.03 μB/Å^3.

Table 3: The magnetic energy ΔE_M, band gap E_g, and total magnetic moment μ of the pristine systems with mono vacancy. NM stands for nonmagnetic/no magnetic moment.

System	Defect	ΔE_M (meV)	E_g (eV)	μ (μ_B)
C_{162}	pristine	−3.2	semi-metal	NM
C_{161}	VC	77.5	metallic	0.4
$B_{81}N_{81}$	pristine	0.4	4.59	NM
$B_{80}N_{81}$	VB	381.4	0.30	1
$B_{81}N_{80}$	VN	128.9	1.79	1

localized magnetic moment (0.4 μ_B). Similarly the Fermi energy decreases for a B vacancy in h-BN sheet (Fig. 1e). However, a N vacancy causes to an increase in E_F (Fig. 1f). In both cases, we notice that

the vacancy defect introduces flat states close to E_F. Flat band nature of these populated states around Fermi level indicates that induced magnetic moment is localized. h-BN with N vacancy is a p-type semiconductor with a band gap of 1.79 eV. Site projected band structure calculations and spin density plot for N vacancy given in Fig. 1i indicate that these states have mainly π characters and magnetic moment is originating from all of the initial bonding B atoms. Magnetization energy values shows that spin polarization for B vacancy in h-BN is highly stable due to external thermal fluctuations with a few hundreds meV value for ΔE_M.

3.4. h-BN Hexagonal Island in Graphene Layout

The ground state geometries of GBN hybrids, an hexagonal shaped island embedded, are presented in Fig. 2. The smallest island both in h-BN and graphene layouts contains one hexagon, whereas the largest one
contains 19 hexagons.

Figure 2. Optimized geometries for Xh-BN(H)@G hybrid nanosheets (see Table 4). Dark blue, light blue, and red colors respectively show C, B, and N atoms.

Our numerical results are summarized in Table 4. The island does not induce any magnetic moment. This nonmagnetic behavior of hybrids involving an h-BN or a graphene hexagonal island is consistent with the literature [30].

Table 4: The magnetic energy ΔE_M, band gap E_g, and total magnetic moment values of GBN hybrids having a hexagonal (H) island. NM stands for nonmagnetic/no magnetic moment.

Hybrid	Name	ΔE_M (meV)	E_g (eV)	μ (μ_B)
$C_{156}B_3N_3$	1h-BN(H)@G	−18.0	0.17	NM
$C_{138}B_{12}N_{12}$	7h-BN(H)@G	−19.0	0.47	NM
$C_{108}B_{27}N_{27}$	19h-BN(H)@G	0.4	0.82	NM

We observe that all hybrids with hexagonal islands exhibit semiconducting behavior. While the energy gap of Xh-BN(H)@G hybrids increases remarkably with increasing X, their Fermi energy, E_F, decreases with X.
Calculated band gaps are all direct as reported in literature [31]. Here we properly show that the hexagonal h-BN island opens up a band gap in the graphene lattice; and that E_g increases with BN concentration. As is seen in Table 1, the formation energies could be even exothermic (negative ε_{fmin} values). One can suggest that the increasing island size does not primarily contribute to the stability of the system. Instead of the island size X, the number of atoms at the interfaces play a decisive role in the stability and electronic properties of GBN hybrids.

3.5. h-BN Hexagonal Island in Graphene Layout with Mono Vacancy

Number of studied pristine hybrids is 3 and the respective C-B bonds/C-N bonds ratios are 3/3, 6/6, and 9/9 for X= 1, 7, and 19 in these Xh-BN(H)@G systems. We totally analyzed 19 in-plane defective hybrids (Xh-BN(H-VY)@G) through the DFT method. Letter X represents the number of hexagons contained by the island, meanwhile letter H inside the parentheses defines the geometrical shape of the island as in hexagonal geometry. Letter V represents mono vacancy in the relevant layout, meanwhile letter Y defines the location of the vacancy.

We examined three different vacancy locations as Interface, Layout and Island and at total ten possibilities with notations of VC_{I1}, VC_{I2}, VC_L, VC_i, VB_I, VB_L, VB_i, VN_I, VN_L, VN_i. A carbon mono vacancy at the interface, $VC_{Interface1}$ ($VC_{Interface2}$), was formed by removing a C atom bonding to two C atoms and a B (an N) atom. We further created a carbon mono vacancy, VC_{Layout} (VC_{island}), by removing a C atom in the graphene layout (graphene island). Respective boron (nitrogen) mono vacancies at the interface and in the layout are designated as $VB_{Interface}$ ($VN_{Interface}$) and VB_{Layout} (VN_{Layout}). We additionally formed B and N mono vacancy in the h-BN island which are signified as VB_{island} and VN_{island} respectively.

Table 5: The magnetic energy ΔE_M, band gap E_g, and total magnetic moment μ of the pristine and defective GBN hybrids having an h-BN hexagonal island. NM stands for nonmagnetic/no magnetic moment.

Hybrid	Defect	ΔE_M (meV)	E_g (eV)	μ (μ_B)
$C_{156}B_3N_3$	pristine	−17.5	0.17	NM
$C_{156}B_2N_3$	VB_I	13.6	metallic	NM
$C_{155}B_3N_3$	VC_{I1}	28.4	metallic	NM
$C_{155}B_3N_3$	VC_{I2}	111.2	metallic	0.06
$C_{155}B_3N_3$	VC_L	77.1	metallic	0.5
$C_{156}B_3N_2$	VN_I	13.1	metallic	1
$C_{138}B_{12}N_{12}$	pristine	−19.4	0.47	NM
$C_{138}B_{11}N_{12}$	VB_i	288.7	metallic	2
$C_{138}B_{11}N_{12}$	VB_I	−4.5	metallic	NM
$C_{137}B_{12}N_{12}$	VC_{I1}	67.4	0.31	NM
$C_{137}B_{12}N_{12}$	VC_{I2}	426.9	metallic	NM
$C_{137}B_{12}N_{12}$	VC_L	136.6	metallic	1.4
$C_{138}B_{12}N_{11}$	VN_i	24.3	metallic	1
$C_{138}B_{12}N_{11}$	VN_I	−3.3	metallic	0.8
$C_{108}B_{27}N_{27}$	pristine	0.4	0.82	NM
$C_{108}B_{26}N_{27}$	VB_i	537.8	metallic	2
$C_{108}B_{26}N_{27}$	VB_I	8.2	0.79	0.7
$C_{107}B_{27}N_{27}$	VC_{I1}	63.5	0.55	NM
$C_{107}B_{27}N_{27}$	VC_{I2}	35	metallic	1
$C_{107}B_{27}N_{27}$	VC_L	439.4	metallic	2
$C_{108}B_{27}N_{26}$	VN_i	54.8	metallic	1
$C_{108}B_{27}N_{26}$	VN_I	3.4	metallic	NM

Our numerical results are summarized in Table 5. The relaxed GBN nanosheets preserve their 2D planar geometry with small local in-plane distortions. Structural
reorganizations was not observed. In general, all hybrids including a mono vacancy exhibit metallic behavior irrespective of their vacancy type and in few cases shrink their own band gap energy E*g* respective to pristine one. The hybrid involving the smallest h-BN island acquires a metallic feature for all types of mono vacancy. On the other hand, the hybrid embracing bigger islands preserves its semiconducting feature whenever a C_{I1} mono vacancy resides and also the hybrid with largest island also preserves that at B_I. In case of pristine GBN hybrids are semiconductors with small band gaps and do not posses any magnetic moment, vacancies make some of the hybrids metallic and magnetic with modest amount of magnetic moments.

Defective hybrid with one single hexagon (1h-BN(HV)@G) exhibit either small or likely unstable magnetization with respect to magnetization energy criterion. The defect VC_L produces very similar ΔE_M, μ values and band structure diagram with the defective graphene sheet indicating decoupling of the island and carbon vacancy. Fermi level decreases by any type vacancies except nitrogen vacancy. This decrease leads systems to have a metallic state as seen in Fig. 3a for electronic band structure of VC_{I2}. The energy band diagram of 1h-BN(H-VN*I*)@G is depicted in Fig. 3b. Increase in E_F, populated states due to dangling bonds around and spin splitting can be clearly seen. Energy bands close to the Fermi energy are nearly flat indicating localization. Only reasonably stable 1h-BN(H-V)@G hybrid exhibit a very small magnetism.

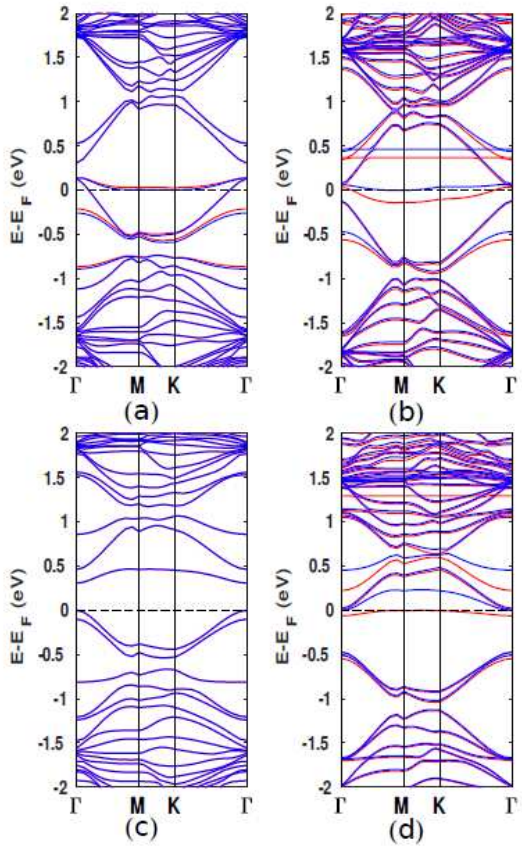

Figure 3. All electronic band structures are spin polarized. (a) 1h-BN(H-VC_{I1})@G, (b) 1h-BN(H-VN_I)@G, (c) 7h-BN(H-VC_{I1})@G, (d) 7h-BN(H-VN_I)@G. The energy bands of spin up electrons are shown in red and those of spin down electrons are in blue. Horizontal
dashed line is the Fermi level.

The highest magnetic moment is obtained in the system with boron vacancy inside the island (VB*I*) for 7h-BN(H-V)@G GBN hybrids. Calculated magnetization energy is quite high indicating to a stable magnetism. Spin polarized electronic band structure of 7h-BN(HVC_{I1})@G is depicted in Fig. 3c. Band gap is clearly seen. Nitrogen removal from the island results as a nonspin polarized system but with a very small ΔE_M value. This system posses magnetic moment value of 0.8 μ_B and nearly flat states near E_F (see Fig. 3d). These states are due to dangling bonds and site projected band structure calculations indicate that these states have mainly π character originating from dangling boron atoms.

4. Conclusion

Energetics of implantation, defect formation, electronic,
and magnetic properties of graphene-h-BN (GBN) 2D planar hybrids is analyzed through the DFT method. Formation energies could be even exothermic (negative ε_{fmin} values). All relaxed GBN hybrids we studied here preserve their 2D planar geometry. Nonmagnetic ground states of hybrids

including a hexagonal island display semiconducting properties. Their energy gaps E_g increase with increasing island size in the graphene layout. We suggest that increasing the stability mainly depends on the number of atoms at the interface rather than the size of island.

Effects of mono vacancies on the structural parameters, electronic and magnetic properties of GBN hybrids are further investigated. It seems to be possible that the nonmagnetic GBN hybrid can attain a stable magnetism when it includes a C, B or an N mono vacancy. Vacancies introduces some localized states (flat bands) and make some of the hybrids metallic and magnetic with modest amount of magnetic moments.

Acknowledgments

This work is supported by The Scientific and Technological Research Council of Turkey (TÜBİTAK)
through the project No: 114F426. Our numerical calculations were performed at TÜBİTAK ULAKBİM, High Performance and Grid Computing Center (TRUBA resources).

References

[1] M. Xu, T. Liang, M. Shi, and H. Chen, Graphene-Like Two-Dimensional Materials, Chemical Reviews, vol. 113, no. 5, pp. 3766-3798, 2013.
[2] K. S. Novoselov, a. K. Geim, S. V. Morozov, D. Jiang, Y. Zhang, S. V. Dubonos, I. V. Grigorieva, and a. a. Firsov, Electric field effect in atomically thin carbon films, Science, vol. 306, no. 5696, pp. 666-669, 2004.
[3] L. Song, L. Ci, H. Lu, P. B. Sorokin, C. Jin, J. Ni, A. G. Kvashnin, D. G. Kvashnin, J. Lou, B. I. Yakobson, and P. M. Ajayan, Large scale growth and characterization of atomic hexagonal boron nitride layers, Nano Letters, vol. 10, no. 8, pp. 3209-3215, 2010.
[4] Y. W. Son, M. L. Cohen, and S. G. Louie, Energy gaps in graphene nanoribbons, Physical Review Letters, vol. 97, no. 21, p. 216803, 2006.
[5] D. C. Elias, R. R. Nair, T. M. G. Mohiuddin, S. V. Morozov, P. Blake, M. P. Halsall, A. C. Ferrari, D. W. Boukhvalov, M. I. Katsnelson, A. K. Geim, and K. S. Novoselov, Control of graphene's properties by reversible hydrogenation: Evidence for graphane, Science, vol. 323, no. 5914, pp. 610-613, 2009.
[6] R. P. Tiwari and D. Stroud, Tunable band gap in graphene with a noncentrosymmetric superlattice potential, Physical Review B, vol. 79, p. 205435, 2009.
[7] S.M. Kim, A. Hsu, P. T. Araujo, Y.-H. Lee, T. Palacios, M. Dresselhaus, J.-C. Idrobo, K. K. Kim, and J. Kong, Synthesis of patched or stacked graphene and hbn flakes: a route to hybrid structure discovery, Nano Letters, vol. 13, no. 3, pp. 933-941, 2013.
[8] L. Ci, L. Song, C. Jin, D. Jariwala, D. Wu, Y. Li, A. Srivastava, Z. F. Wang, K. Storr, L. Balicas, F. Liu, and P. M. Ajayan, Atomic layers of hybridized boron nitride and graphene domains, Nature Materials, vol. 9, no. 5, pp. 430-435, 2010.
[9] D. J. Appelhans, Z. Lin, and M. T. Lusk, Two-dimensional carbon semiconductor: Density functional theory calculations, Physical Review B, vol. 82, no. 7, p. 073410, 2010.
[10] X. R. Wang, X. L. Li, L. Zhang, Y. Yoon, P. K. Weber, H. L. Wang, J. Guo, and H. J. Dai, N-doping of graphene through electrothermal reactions with ammonia, Science, vol. 324, no. 5928, pp. 768-771, 2009.
[11] A. Quandt, C. Özdoğan, J. Kunstmann, and H. Fehske, Boron doped graphene nanostructures, Physica Status Solidi B, vol. 245, no. 10, pp. 2077-2081, 2008.
[12] A. Quandt, C. Özdoğan, J. Kunstmann, and H. Fehske, Functionalizing graphene by embedded boron clusters, Nanotechnology, vol. 19, no. 33, p. 335707, 2008.
[13] C. Özdoğan, J. Kunstmann, and A. Quandt, Localization of metallicity and magnetic properties of graphene and of graphene nanoribbons doped with boron clusters, Philosophical Magazine, vol. 94, no. 16, pp. 1841-1858, 2014.
[14] X. Fan, Z. Shen, A. Q. Liu, and J.-L. Kuo, Band gap opening of graphene by doping small boron nitride domains, Nanoscale, vol. 4, no. 6, pp. 2157-2165, 2012.
[15] Q. Peng and S. De, Tunable band gaps of mono-layer hexagonal bnc heterostructures, Physica E, vol. 44, no. 7-8, pp. 1662-1666, 2012.
[16] T. P. Kaloni, R. P. Joshi, N. P. Adhikari, and U. Schwingenschl ¨ogl, Band gap tunning in bn-doped graphene systems with high carrier mobility, Applied Physics Letters, vol. 104, no. 7, pp. 073116-5, 2014.
[17] B. Muchharla, A. Pathak, Z. Liu, L. Song, T. Jayasekera, S. Kar, R. Vajtai, L. Balicas, P. M. Ajayan, S. Talapatra, and N. Ali, Tunable electronics in large-area atomic layers of boron-nitrogen-carbon, Nano Letters, vol. 13, no. 8, pp. 3476-3481, 2013.
[18] H. I. Rasool, C. Ophus, and A. Zettl, Atomic Defects in Two Dimensional Materials, Advanced Materials, vol. 27, no. 38, pp. 5771-5777, 2015.
[19] Y. Zhang, S.-Y. Li, H. Huang, W.-T. Li, J.-B. Qiao, W.-X.Wang, L.-J. Yin, K.-K. Bai, W. Duan, and L. He, Scanning tunneling microscopy of the π magnetism of a single carbon vacancy in graphene, Physical Review Letters, vol. 117, p. 166801, 2016.
[20] W. Kohn and L. Sham, Self-consistent equations including exchange and correlation effects, Physical Review, vol. 140, no. 4A, pp. 1133-1138, 1965.
[21] J. P. Perdew and Y. Wang, Accurate and simple analytic representation of the electron-gas correlation energy, Physical Review B, vol. 45, no. 23, pp. 13244-13249, 1992.
[22] J. P. Perdew, J. A. Chevary, S. H. Vosko, K. A. Jackson, M. R. Pederson, D. J. Singh, and C. Fiolhais, Atoms, molecules, solids, and surfaces: Applications of the generalized gradient approximation for exchange and correlation, Physical Review B, vol. 46, p. 6671, 1992.
[23] G. Kresse and J. Furthmuller, Efficiency of ab-initio total energy calculations for metals and semiconductors using a planewave basis set, Computational Materials Science, vol. 6, no. 1, pp. 15-50, 1996.

[24] G. Kresse and J. Furthmuller, Efficient iterative schemes for ab initio total-energy calculations using a plane-wave basis set, Physical Review B, vol. 54, no. 16, pp. 11169-11186, 1996.
[25] P. E. Blochl, O. Jepsen, and O. K. Andersen, Improved tetrahedron method for brillouin-zone integrations, Physical Review B, vol. 49, no. 23, pp. 16223-16233, 1994.
[26] G. Kresse and D. Joubert, From ultrasoft pseudopotentials to the projector augmented-wave method, Physical Review B, vol. 59, no. 3, pp. 1758-1775, 1999.
[27] C. Özdoğan, S. Mukhopadhyay, W. Hayami, Z. B. Güvenç¸, R. Pandey, and I. Boustani, The unusually stable b-100 fullerene, structural transitions in boron nanostructures, and a comparative study of alpha- and gamma-boron and sheets, Journal of Physical Chemistry C, vol. 114, no. 10, pp. 4362-4375, 2010.
[28] R. W. G. Wyckoff, Crystal Structures, vol. 1 of Crystal Structures. New York: Interscience Publishers, second ed., 1963.
[29] N. Akman and C. Özdoğan, Island shape, size and interface dependency on electronic and magnetic properties of graphene hexagonal-boron nitride (h-bn) in-plane hybrids, Journal of Physics and Chemistry of Solids, vol. 115, pp. 187-198, 2018.
[30] Y. Liu, S. Bhowmick, and B. I. Yakobson, Bn white graphene with colorful edges: the energies and morphology, Nano Letters, vol. 11, no. 8, pp. 3113-3116, 2011.
[31] P. P. Shinde and V. Kumar, Direct band gap opening in graphene by BN doping: Ab initio calculations, Physical Review B, vol. 84, no. 12, p. 125401, 2011.